The Meteoritical Society

Meteoritics & Planetary Science 52, Nr 2, 197–205 (2017)
doi: 10.1111/maps.12788

Thermophysical properties of Almahata Sitta meteorites (asteroid 2008 TC_3) for high-fidelity entry modeling

Stefan LOEHLE[1,*], Peter JENNISKENS[2,3], Hannah BÖHRK[4], Thomas BAUER[5], Henning ELSÄβER[4], Derek W. SEARS[3], Michael E. ZOLENSKY[6], and Muawia H. SHADDAD[7]

[1]High Enthalpy Flow Diagnostics Group, Institute of Space Systems, 70569 Stuttgart, Germany
[2]SETI Institute, Carl Sagan Center, Mountain View, California 94043, USA
[3]NASA Ames Research Center, Mountain View, California 94035, USA
[4]DLR, Institute of Structures and Design, 70569 Stuttgart, Germany
[5]DLR, Institute of Technical Thermodynamics, 51147 Cologne, Germany
[6]ARES, NASA Johnson Space Center, Houston, Texas 77058, USA
[7]Physics Department, University of Khartoum, Khartoum, Sudan
[*]Corresponding author. E-mail: loehle@irs.uni-stuttgart.de

(Received 14 December 2015; revision accepted 15 September 2016)

Abstract–Asteroid 2008 TC_3 was characterized in a unique manner prior to impacting Earth's atmosphere, making its October 7, 2008, impact a suitable field test for or validating the application of high-fidelity re-entry modeling to asteroid entry. The accurate modeling of the behavior of 2008 TC_3 during its entry in Earth's atmosphere requires detailed information about the thermophysical properties of the asteroid's meteoritic materials at temperatures ranging from room temperature up to the point of ablation ($T \sim 1400$ K). Here, we present measurements of the thermophysical properties up to these temperatures (in a 1 atm. pressure of argon) for two samples of the Almahata Sitta meteorites from asteroid 2008 TC_3: a thick flat-faced ureilite suitably shaped for emissivity measurements and a thin flat-faced EL6 enstatite chondrite suitable for diffusivity measurements. Heat capacity was determined from the elemental composition and density from a 3-D laser scan of the sample. We find that the thermal conductivity of the enstatite chondrite material decreases more gradually as a function of temperature than expected, while the emissivity of the ureilitic material decreases at a rate of 9.5×10^{-5} K^{-1} above 770 K. The entry scenario is the result of the actual flight path being the boundary to the load the meteorite will be affected with when entering. An accurate heat load prediction depends on the thermophysical properties. Finally, based on these data, the breakup can be calculated accurately leading to a risk assessment for ground damage.

INTRODUCTION

Since a 20-m-sized meteoroid that impacted near Chelyabinsk generated an airburst that sent over 1600 people to the hospital for medical treatment of glass cuts (Popova et al. 2013), the potential damaging consequences of the impact of small 10- to 100-m-sized asteroids have been taken more seriously. Efforts are underway to predict these impacts in some detail with respect to the breakup and strewn field on the ground using computing tools originally developed for the reentry of spacecraft and the development of thermal protection systems (Arnold et al. 2015). For such work, as much as possible needs to be known about the initial shape and orientation of the asteroid during impact. In addition, detailed thermophysical properties of the relevant materials need to be known at temperatures well above room temperature (Jones and Kaiser 1966).

Asteroid 2008 TC_3 was observed in space before impacting over the Nubian desert of Sudan on October 7, 2008 (Jenniskens et al. 2009). The impact was observed from space (Borovicka and Charvat 2009). The shape and orientation of the asteroid during impact

were determined from asteroid light curve analysis (Scheirich et al. 2010). This makes 2008 TC_3 a unique test case for validating the application of high-fidelity reentry modeling of small asteroid impacts. Re-entry modeling has been used to calculate the flowfield around spacecraft re-entering Earth's atmosphere and determines the heat load to the structure by calculating the convective, conductive, and radiative heat transfer. The resulting heat load to the structure depends on the thermophysical properties of the heat shield material. For a meteorite entry, the same tools could be applied if the thermophysical properties of the meteorite are available.

The recovered meteorites can be used to measure the relevant thermophysical properties of the material. Some 600 meteorites from the Almahata Sitta fall were found at documented locations on the ground (Jenniskens et al. 2009; Shaddad et al. 2010). Most recovered meteorites were ureilites, but 20–30% were a variety of more than 10 different types of enstatite and ordinary chondrites (Zolensky et al. 2010; Bischoff et al. 2010). The fallen material is collectively referred to as a single meteorite called Almahata Sitta (AhS), which is classified as an anomalous polymict ureilite. Based on other known polymict ureilites, it is suspected that the nonureilitic materials survived entry more efficiently and most of the initial asteroid was composed of ureilites, with perhaps 1–2% of enstatite and ordinary chondrites mixed in (Goodrich et al. 2015).

Of key interest are the thermal conductivity and the specific heat capacity of all these materials. Heat capacity is defined as the heat required to change the temperature of unit mass of a substance by one unit of temperature. Thermal conductivity is the material's ability to transport heat or packages of vibrational energy called phonons. Of interest too is the emissivity of these materials, their effectiveness in emitting energy as thermal radiation, often expressed as the spectral hemispherical emissivity in wavelength (ε_λ) being the fraction emitted of the expected blackbody radiation at that temperature.

For the modeling of an asteroid entry in Earth's atmosphere, such information is required for temperatures well above room temperature, until the point of melting. Detailed thermal conductivity and emissivity measurements were made of various minerals in the past (e.g., Robie et al. 1978), but so far meteoritic materials have only been studied at room temperatures and below, relevant for the study of the Yarkovsky and YORP effects (thermal inertia) on asteroids in space and the sublimation rate of comets and other icy bodies (thermal diffusivity) (Yomogida and Matsui 1983; Matsui and Osako 1979; Parthasarathy and Sharma 2004; Opeil et al. 2010, 2012; Wach et al. 2014).

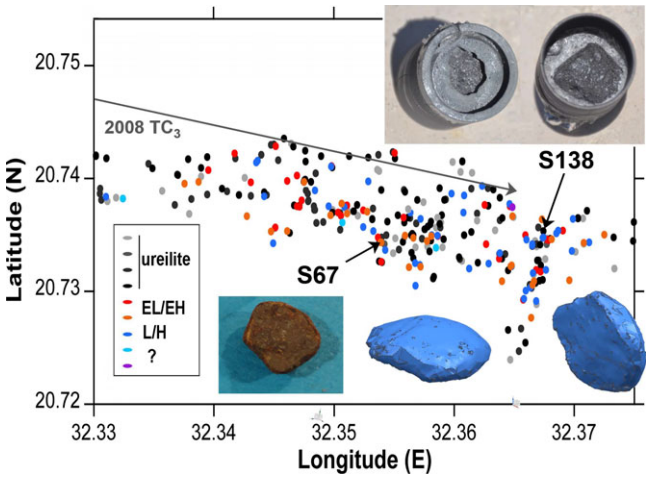

Fig. 1. Almahata Sitta meteorites S67 and S138 and their position in the strewn field. The ground-projected trajectory of 2008 TC_3 is that according to Farnocchia (unpublished data). Positions of recovered meteorites are color coded by meteorite type (see legend) according to a preliminary classification based on visual inspection of the meteorites by Shaddad et al. (2010). The lower insets show a photo of S67 and 3-D scans of this meteorite. The upper inset shows the front and back of S138 after emissivity testing. (Color figure can be viewed at wileyonlinelibrary.com.)

Here, we present data on the thermophysical properties of two samples from the AhS meteorite. Sample AhS S138 is a ureilite described in Zolensky et al. (2010). Sample AhS S67 is an EL6 chondrite similar to a previously examined AhS sample studied by Zolensky et al. (2010). AhS S138 was suitable shaped for emissivity measurements, and AhS S67 was suitable shaped for thermal diffusivity measurements. Measurements were made at temperatures 300–1200 K.

SAMPLES AND EXPERIMENTAL PROCEDURES

The two Almahata Sitta meteorites studied here are from the University of Khartoum collection. The location of these meteorites in the strewn field is shown in Fig. 1. Meteorite AhS S67 was typed as EL6, and its mineral composition was determined using the Cameca SX100 electron microprobe (EPMA) at the E-beam laboratory of the Astromaterials and Exploration Science Directorate, Johnson Space Center, using a thin section made from the surface area after diffusivity measurement. We made point analyses at 15 kV and used natural mineral standards. The composition of critical minerals in sample S67 was measured in two electron microprobe runs, both of which are summarized in Table 1. The values are mean values of two different data sets with 100 and 80 measurement points, respectively. The material was rich in opaque minerals. Low Ca pyroxene had average composition

Table 1. The mean of elemental heat capacities determined from individual positions in the meteorite and the mean weight% for S67. Because metallic iron and troilite are not in the form of oxides, the total weight% adds up to more than 100.

Element	Heat capacity J (kg^{-1} K^{-1}) T = 300 K	Weight% in S67 Data set 2	Weight% in S67 Data set 3
Na	1228	0.27	0.51
S	736	4.20	2.85
P	669	0.06	0.05
K	753	0.03	0.07
Mg	1017	12.58	11.56
Al	900	0.71	1.57
Si	703	19.32	22.13
Ca	653	0.24	0.44
Ti	522	0.04	0.02
Fe	450	28.30	21.70
Cr	449	0.29	0.13
Mn	479	0.05	0.04
Co	421	0.08	0.06
Ni	444	2.32	1.78
O	918	44.34	44.30
Sum		112.84	107.21
From average composition: <C_p (J kg^{-1} K^{-1}) —300 K>		756 ± 124	776 ± 127
No. of samples		100	80
Mean of individual positions: C_p (J kg^{-1} K^{-1}) —300 K		688 ± 113	670 ± 113

$Fo_{97.9}$ $Wo_{0.2}$ or $Fa_{1.9}$ $Wo_{0.2}$, while troilite has up to 2.78 atom% Cr. Some metallic iron was analyzed during the probe session. AhS S67 is typical of a large number of enstatite chondrites found in the southern part of the strewn field. It is a small 1-cm-sized cap (695.23 mg, about 3.57 mm thick) of a larger oriented meteorite (Fig. 1). Its flat broken surface and the homogeneous thickness made this sample particularly suitable for thermal diffusivity measurements.

A 3-D model of AhS S67 was derived using a 3-D laser scanner (see inset in Fig. 1). These data were used to determine the volume of the fragment as 207.2 mm^3, resulting in a density for the fragment of ρ = 3.35 g cm^{-3} (±0.02). The surface was slightly flattened to facilitate the diffusivity measurement, so the density value could be a little smaller. Indeed, a density of ρ = 3.16 (+0.12/−0.06) g cm^{-3} was measured for EL6 chondrite Almahata Sitta sample 41 (Shaddad et al. 2010).

AhS S138 measures about 1 × 1 × 2 cm in size and is a coarse-grained ureilite (Fig. 1). Most of asteroid 2008 TC_3 is thought to have been composed of ureilitic material with composition similar to that of S138 (Goodrich et al. 2015). With a flat front surface, the size and shape of this meteorite is ideal for emissivity measurements. The composition of this meteorite was not measured.

Thermal Diffusivity Measurement

Thermal diffusivity measurements were made using the laser flash method, with the sample placed in an inert argon atmosphere. The warming induced by a laser heat flash on one side is measured with an IR camera on the backside of the sample. A commercial LFA 457 MicroFlash device was used that was able to heat the sample to 1100 °C. The sample itself is kept in an isothermal environment at the temperature level of interest before a laser flash is triggered.

The sample is heated very quickly with a laser pulse at the front side (from bottom to top in Fig. 2). The temporal evolution of temperature on the rear side of the sample is observed using an infrared camera. It is assumed that the heat conduction process through the sample is 1-D. The heat equation in one dimension (x) is as follows:

$$\frac{\partial T}{\partial t} = \alpha \frac{\partial^2 T}{\partial x^2} \tag{1}$$

Inside the sample, the temperature distribution is described by the solution of this heat equation with the following two boundary conditions: a short heat pulse Q (the *laser* flash) on one side and thermal insulation at the opposite end (x = l). Parker et al. (1961) first published this method. The temperature distribution is as follows:

$$T(l,t) = \frac{Q}{\rho\, c\, l}\left[1 + 2\sum_{n=0}^{\infty}(-1)^n e^{\frac{-n^2\pi^2}{l^2}\alpha t}\right] \tag{2}$$

Figure 3 shows the development over time of the temperature at the rear end of the sample. The temperature is normalized to its maximum and the abscissa is the dimensionless time ω.

The thermal diffusivity

$$\alpha = \frac{\lambda}{\rho c} \tag{3}$$

of the sample is measured at the time $t_{1/2}$ required for the back side of the sample to reach half the maximum temperature, i.e.,

$$a = 1.38\ \frac{l^2}{\pi^2 t_{1/2}} \tag{4}$$

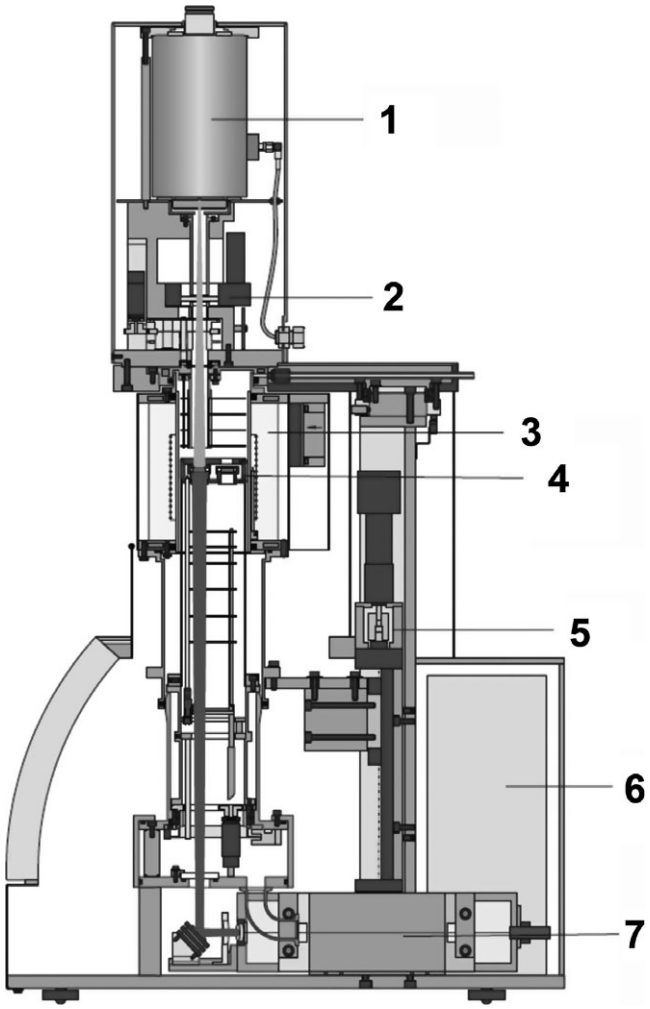

Fig. 2. Thermal diffusivity measurement facility with (1) detector; (2) iris, (3) furnace, (4) sample carrier, (5) furnace hoist, (6) electronics, and (7) laser.

In order to measure the thermal diffusivity, it is, therefore, sufficient to know the temperature rise from the heat pulse and the sample's thickness. Note that the absolute value of the heat pulse is not required. The applied method for the analysis of the S67 follows this approach taking into account the boundary losses through radiation at the front side as presented by Cape and Lehman (1963). The sample was flattened at the side toward the laser flash, which had a duration of 0.5 ms. Any systematic uncertainty due to the inhomogeneous thickness is considered to be ±30%.

Specific Heat Capacity

The specific heat capacity of a material is depending on the capability of a material to store energy. Therefore, for a composite material, the effective specific heat capacity depends on the composition of the material:

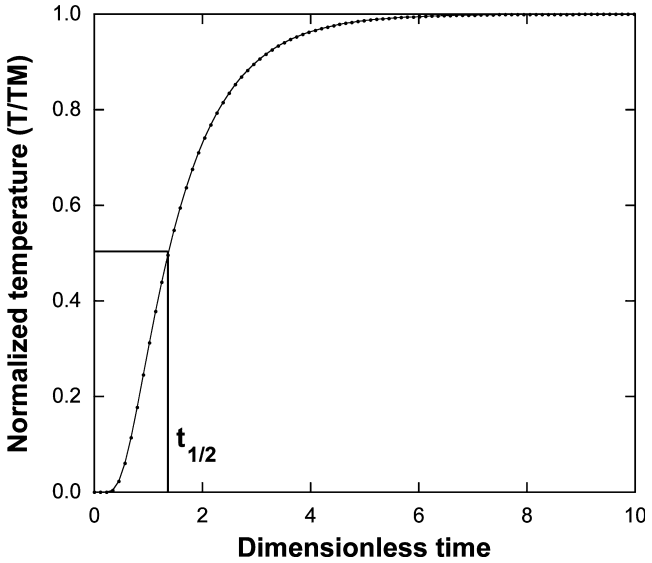

Fig. 3. Theoretical temporal evolution of the rear-side temperature, expressed in terms of dimensionless time ($\omega = \pi^2/l^2 \propto t$) and normalized temperature to the mean value of the temperature range T/T_M.

$$C_p = \sum \xi_i * c_{p,i} \quad (5)$$

where ξ_i stands for the mass fraction of the element and $c_{p,i}$ is the specific heat capacity of the element at room temperature. The bulk elemental composition of the sample was used to derive the specific heat capacity at room temperature. The derived value is C_p, because the pressure during testing was constant, while the volume could change and mass loss shows that there is a small change.

Emissivity Measurement

The emissivity was measured using the emissivity measurement facility (EMF) at the Institute of Space Systems of the University of Stuttgart. The facility is described in detail in Schuessler et al. (2009). Figure 4 shows the facility and the functional elements. The sample is placed deep in a graphite tube (Fig. 4C). Inside the tube, it is radiating as a blackbody in an inert argon atmosphere, with emissivity $0.9993 < \varepsilon \leq 1.0000$. The sample is then quickly (isothermally) moved to the front by a piston, where it radiates with emissivity typical of that particular meteorite sample. If the movement is fast enough, the temperature will not have changed. The transition time in the facility is ~0.2 s. The surface temperature and graybody emission of the heated sample are measured using a spectrally integrating GIRL IM-5 pyrometer with a spectral response in between 1.1 and 22 μm. This pyrometer is mounted in front of the long tube. The temperature is

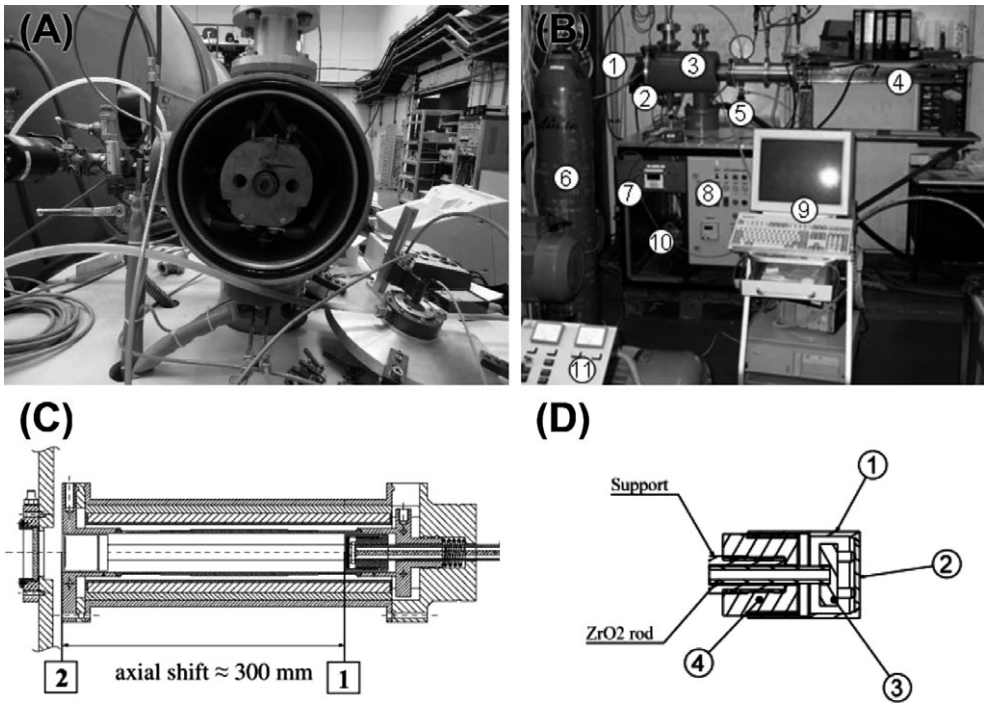

Fig. 4. Emissivity measurement facility (EMF). A) Mounted meteorite fragment in front position with open front lid. B) Facility overview, with (1) pyrometer, (2) cooled access window, (3) vacuum tank, (4) pneumatic cylinder, (5) DC power supply, (6) argon supply, (7) pyrometer electronics, (8) measurement control unit, (9) data monitoring and acquisition system, (10) two-stage vacuum system, and (11) power control unit. C) Mounting tube with (1) sample holder, (2) sample, (3) guide plate, (4) sample support. D) Detail of sample holder, with (1) sample holder, (2) sample, (3) insulator, (4) sample rod.

measured through a water-cooled KRS-5 window, which has a known spectral transmissivity of 69.0 ± 0.5% at 700 nm, increasing to 72.0 ± 0.5% at 30 μm. The temperature measurement is obtained after correcting for spectral response, which is a combination of the window transmission and the IM-5 spectral responsivity.

In particular, the movement of the sample is so quick that the sample stays isothermal. Thus, a measured temperature change in the front position is only due to the change from the blackbody emissivity (taken as $\varepsilon = 1$ in position 1) to the material's emissivity at this temperature level (in position 2). The emissivity can, therefore, be determined directly from the measured temperatures in the two positions as follows:

$$\varepsilon = \frac{T_2^4}{T_1^4}, \tag{6}$$

where T_1 and T_2 stand for the temperature in the back and the front position, respectively. More details of the procedure and the facilities are described in Schuessler et al. (2009). The quality of the measurements in this facility have been investigated in the past by round robin testing with data from several metrological institutes (Monte et al. 2011).

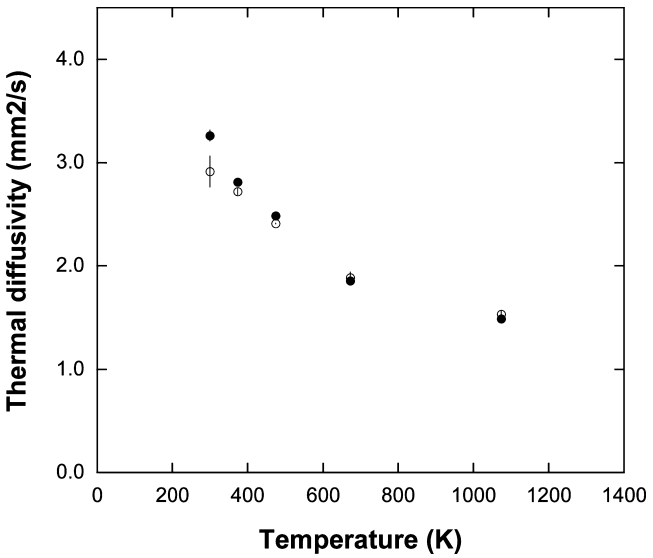

Fig. 5. Thermal diffusivity measurement of sample S67. Error bars show the random measurement uncertainty only, the systematic uncertainty due to the unknown geometry is ±30%.

RESULTS

Results from thermal diffusivity measurements are shown in Fig. 5. The data comprise two heating runs

Table 2. Thermophysical properties derived from thermal diffusivity measurements of enstatite chondrite S67 along two warming curves (curves I and II).

T (°C)	T (K)	Thermal diffusivity I (10^{-6} m^2 s^{-1})	T (K)	Thermal diffusivity II (10^{-6} m^2 s^{-1})	Thermal conductivity (W m^{-1} K^{-1})
20	299.6 ± 0.2	3.26 ± 0.05	299.5 ± 0.5	2.92 ± 0.15	6.92 ± 2.1
100	373.9 ± 0.5	2.81 ± 0.03	373.9 ± 0.5	2.72 ± 0.03	5.36 ± 1.6
200	474.1 ± 0.5	2.49 ± 0.01	473.9 ± 0.5	2.41 ± 0.01	4.87 ± 1.46
400	673.5 ± 0.2	1.86 ± 0.04	673.5 ± 0.2	1.89 ± 0.05	3.51 ± 1.05
800	1073.3 ± 0.1	1.49 ± 0.04	1073.4 ± 0.2	1.53 ± 0.03	2.92 ± 0.88

with five single laser shots per temperature. Between the two heating runs, the sample was repositioned. Results are in good agreement.

From the composition of S67, the specific heat capacity follows from the thermal diffusivity measurements (see Equation 5). A mean specific heat capacity is calculated from an average of all specific heat capacities following from the compositions of the different measurement locations for the two data sets. A mean of these two data sets results in a mean specific heat capacity for this S67 at room temperature of $c_p = 679 \pm 113$ J kg^{-1} K^{-1}. The accuracy is the mean standard deviation out of the 100 and 80 measurements, respectively.

In the range 300–1100 K, the specific heat capacity is expected to change by only ~150 J kg^{-1} K^{-1} on theoretical arguments (Gosh and McSween 1999). According to the Dulong–Petit law, the molar heat capacity tends to one single value for all elements in the solid phase at higher temperatures because the maximum inner energy i in the vibrational mode of the crystal structure is limited to $i = 3RT$. Toward high temperatures, the value 25 J mol^{-1} K^{-1} should be reached for all species. With the molar weight of 23.96 g mol^{-1}, derived from the measured composition, this translates to $C_p = 1043$ J kg^{-1} K^{-1}, at the state of maximal excitation (@25 J mol^{-1} K^{-1}). The Dulong–Petit law is quite accurate for solids with simple elemental composition. In case of more complex molecular composition, the vibrational energy of the molecules has to be considered leading to higher molar heat capacities.

From the measured EL6 density and the specific heat capacity, the heat conductivity is calculated (Equation 3). Results are summarized in Table 2 and plotted in Fig. 6. The conductivity values are determined under the assumption that the specific heat capacity does not change drastically with temperature.

Figure 7 shows the results of the emissivity measurements from the ureilite S138 as a function of temperature. At each temperature level, two to three measurements have been performed. There is a small difference in temperature between the runs at one

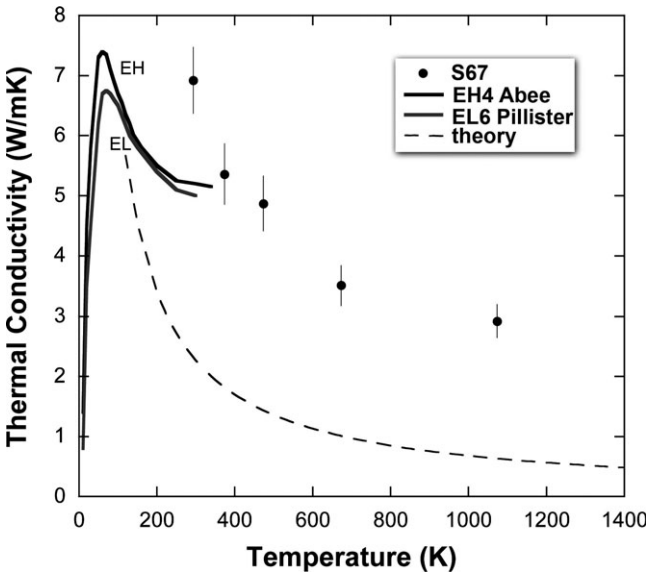

Fig. 6. Thermal conductivity of EL6 chondrite S67, compared to measurements for EH4 chondrite Abee and EL6 chondrite Pillister by Opeil et al. (2010, 2012). Dashed line shows the theoretically expected temperature dependence.

temperature level. This is due to the power regulator of the black body source. The emissivity is decreasing with increasing temperature of the surface at a rate of 9.5×10^{-5} K^{-1} between 777 and 1207 K. The sample melted at 1150 K, which was observed during the heating to 1200 K. The last value in Fig. 7 is possibly influenced by the melting process. From a visual inspection, the sample appears a bit brighter after the tests and is more reflective. The higher reflectivity implies that the emissivity decreased, as measured.

DISCUSSION

Values for comparison for higher temperatures have not been measured elsewhere so far. The thermal diffusivity decreases as a function of temperature (Fig. 6).

The results for specific heat capacity at room temperature (679 ± 113 J kg^{-1} K^{-1}) is higher than the C_p ~ 520 J kg^{-1} K^{-1} value for EL enstatite chondrites

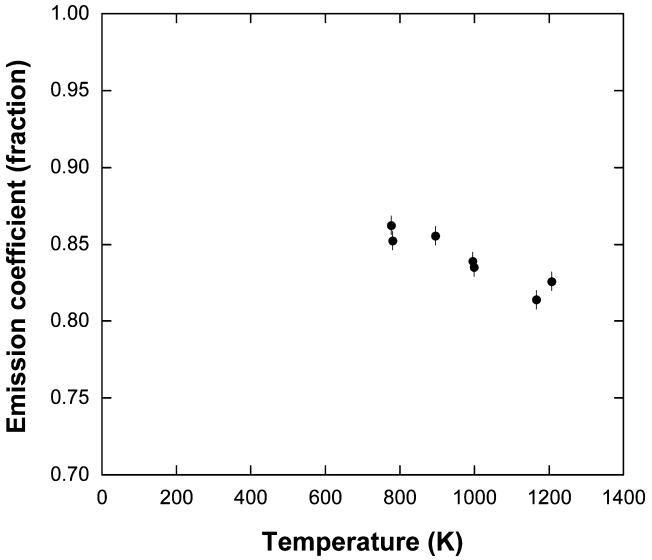

Fig. 7. Emissivity measurement of S138.

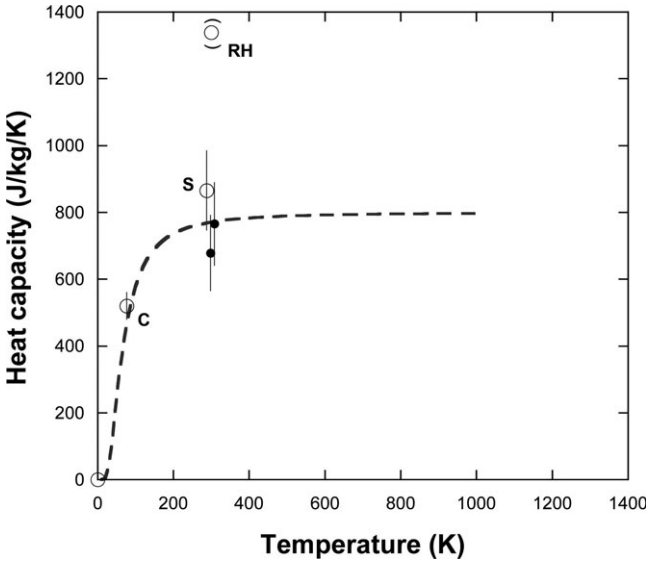

Fig. 8. Estimate of specific heat capacity for EL6 enstatite chondrites (•). Open circles are measurements by calorimetric techniques (Consolmagno et al. 2014 [C]; Rudee and Herndon 1981 [RH]; Szurgot 2011 [S]). The dashed curve is the expected temperature dependence according to Einstein's model if the composition remains unaltered.

measured at 77 K by Macke et al. (2014) and Consolmagno et al. (2014), but lower than the C_p = 1340 J kg^{-1} K^{-1} measured at room temperature by Rudee and Herndon (1981) for EH4 chondrite Abee. The value is close to the C_p = 690 J kg^{-1} K^{-1} at 300 K for the Kilabo LL6 chondrite (Wach et al. 2014) and the average of 866 ± 119 J kg^{-1} K^{-1} measured for stony meteorites by Szurgot (2011) (Fig. 8).

The expected temperature dependence according to the Einstein model of solids is shown by a dashed line in Fig. 8 and expressed simply according to $C_v = A\ (T_E/T)^2\ \exp(T_E/T)/(\exp\ (T_E/T) - 1)^2$, with Einstein temperature $T_E \sim 200$ K and constant $A \sim 800$ J kg^{-1} K^{-1} to match the measured values. The more accurate Debye model deviates only slightly at lower temperatures, but is less simple analytically. The heat is contained in vibrational modes that depend on the material composition and are a function of temperature due to activation energy barriers. The lower value at 77 K (Consolmagno et al. 2013) is on account of the lower excitation of vibrational states and rises to reach a plateau only at 600 K, due to forsterite, enstatite, and anorthite minerals, and it is expected to again rapidly increase above 800 K due to metallic iron (Macke et al. 2014). At 300 K, forsterite, enstatite, and anorthite contribute about 770 J kg^{-1} K^{-1}, fayalite a lower 580 J kg^{-1} K^{-1}, while metalic iron has only 310 J kg^{-1} K^{-1} (Gosh and McSween 1999). The dashed curve in Fig. 8 shows the expected behavior if $C_p = 770 \exp(-32/T)$.

The resulting values for thermal conductivity at room temperature (6.92 W m^{-1}K^{-1}) are higher than presented by Opeil et al. (2010, 2012) for room temperature and lower, but lower than found for EH4 Abee by Rudee and Herndon (1981). The conductivity of samples is often affected by inhomogeneitites in the meteoritic fabric, resulting in lower values than those of pure minerals. Enstatite chondrite Abee (E4) showed no such effect and had values more typical of those of enstatite and olivine minerals (4.5–5 W m^{-1} K^{-1}), in agreement with our enstatite chondrite. The difference in metal content makes only a small difference in thermal conductivity (Fig. 6).

At temperatures below 50 K, the theory for crystalline insulating materials, where heat transport is dominated by phonon transport, predicts that the thermal conductivity is controlled by the phonon activation energy, increasing with T^3 when temperature increases (Opeil et al. 2012). Increased production of phonons results in increased likelihood of scattering, as a result of which the conductivity will decrease proportional to $\lambda_T \sim \exp\ (\theta_D/\alpha T)$, where θ_D is the Debye temperature and α is a constant (Klein 1967). To first order, this is a $\lambda_T \sim 1/T$ dependence. In practice, less steep dependencies are often observed. The thermal conductivity will also depend on the material properties, as phonons will scatter from metal grains, grain boundaries, and isolated pore spaces. For enstatite chondrites, the thermal conductivity is gradually increasing with temperature below 50 K, but that trend reverses above 50 K. At very high temperatures, the thermal conductivity is expected to follow a $\sim 1/T$ dependence. Based on our measurements, the thermal

conductivity decreases less rapidly, following an exponential decay proportional to 6.9 * exp (−0.00092 T(K)).

The factor 2–3 higher thermal conductivity would permit a more rapid transport of heat during atmospheric entry, keeping the surface temperature of the meteoroid lower than otherwise expected. This will lower the rate of ablation and decrease the luminosity of the meteoroid. In contrast, the slightly lower emissivity at high temperatures will increase the surface temperature and increase the rate of ablation.

The lower emissivity at temperatures above 900 K will slightly decrease the rate at which energy is radiated and the surface is cooled at these high temperatures. This temperature dependence is observed more often for dark materials, with emissivity initially increasing as a function of temperature, then decreasing after reaching a peak. Emissivity is a function of wavelength and the specific value depends on the wavelength range considered here (1.1–22 μm). The gray body radiation of the tested meteorites falls within this wavelength range. Therefore, the measurements are considered to be spectrally integrated emissivity values.

Both the emissivity of ureilitic materials and the thermal conductivity of enstatite chondrite materials decrease as a function of temperature above 500 K. Normally, thermal conductivity and emissivity behave in an inverse manner. In metals, emissivity increases slowly as the metal warms, then increases rapidly approaching melting point. These highly conductive materials have low emissivity at room temperature, but heating will lower the thermal conductivity and increase emissivity. When the material melts, the conductivity drops and emissivity rises rapidly. Nonmetals are poor thermal conductors and start out with high emissivity. When the material warms, electrons become more mobile, the thermal conductivity tends to increase, and the emissivity will decrease.

CONCLUSIONS

The first measurements of specific heat capacity and thermal conductivity for recovered samples of asteroid 2008 TC_3 at temperatures relevant to asteroid entry in Earth's atmosphere are presented. The thermal conductivity of EL6 enstatite chondrite material stays higher than expected above 300 K, with implications for heat transport into the asteroid and the rate of meteoroid ablation. The emissivity of ureilitic material decreases above 900 K, with implications for the efficiency at which heat is radiated from the surface.

Future work will expand on these preliminary measurements by probing a wide range of relevant materials at the temperatures attained during asteroid entry. These data are essential for a reliable prediction of the breakup scenario, the resulting area of impact of fragments and finally the prediction of the risk of damage on ground. The entry scenario is the result of the actual flight path being the boundary to the load the meteorite will be affected with when entering. An accurate heat load prediction depends on the thermophysical properties. Finally, based on these data, the breakup can be calculated accurately leading to a risk assessment for ground damage.

Acknowledgments—P. J. and D. S. acknowledge support from the NASA Ames Research Center's Asteroid Threat Assessment Project and the NASA's Near Earth Object Observation program.

Editorial Handling—Dr. Cyrena Goodrich

REFERENCES

Arnold J. O., Burkhard C. D., Venkapathy E., and Morrison D. 2015. First international workshop on potentially hazardous asteroids characterization, atmospheric entry and risk assessment. July 7–9, 2015. NASA Ames Research Center. http://planetary-defense.arc.nasa.gov/workshop2015/

Bischoff A., Horstmann M., Pack A., Laubenstein M., and Haberer S. 2010. Asteroid 2008 TC_3—Almahata Sitta: A spectacular breccia containing many different ureilitic and chondritic lithologies. *Meteoritics & Planetary Science* 45:1638–1656.

Borovicka J. and Charvat Z. 2009. Meteosat observation of the atmospheric entry of 2008 TC_3 over Sudan and the associated dust cloud. *Astronomy & Astrophysics* 507:1015–1022.

Cape J. A. and Lehman G. W. 1963. Temperature and finite pulse-time effects in the flash method for measuring thermal diffusivity. *Journal of Applied Physics* 34:1909–1913.

Consolmagno G. J., Schaefer M. W., Schaefer B. E., Britt D. T., Macke R. J., Nolan M. C., and Howell E. S. 2013. The measurement of meteorite heat capacity at low temperatures using liquid nitrogen vaporization. *Planetary and Space Science* 87:146–156.

Consolmagno G., Macke R., and Britt D. 2014. Meteorite heat capacities: Results to date. In *Proceedings of Asteroids, Comets, Meteors 2014*. edited by Muinonen K., Penttilä A., Granvik M., Virkki A., Fedorets G., Wilkman O., and Kohout T., Helsinki. Finland: University of Helsinki. 1 p.

Goodrich C. A., Hartmann W. K., O'Brien D. P., Weidenschilling S. J., Wilson L., Michel P., and Jutzi M. 2015. Origin and history of ureilitic material in the solar system: The view from asteroid 2008 TC_3 and the Almahata Sitta meteorite. *Meteoritics & Planetary Science* 50:782–809.

Gosh A. and McSween H. Y. 1999. Temperature dependence of specific heat capacity and its effect on asteroid thermal models. *Meteoritics & Planetary Science* 34:121–127.

Jenniskens P., Shaddad M. H., Numan D., Elsir S., Kudoda A. M., Zolensky M. E., Le L., Robinson G. A., Friedrich

J. M., Rumble D., Steele A., Chesley S. R., Fitzsimmons A., Duddy S., Hsieh H. H., Ramsay G., Brown P. G., Edwards W. N., Tagliaferri E., Boslough M. B., Spalding R. E., Dantowitz R., Kozubal M., Pravec P., Borovicka J., Charvat Z., Vaubaillon J., Kuiper J., Albers J., Bishop J. L., Mancinelli R. L., Sandford S. A., Milam S. N., Nuevo M., and Worden S. P. 2009. The impact and recovery of asteroid 2008 TC_3. *Nature* 458:485–488.

Jones J. and Kaiser T. R. 1966. The effects of thermal radiation, conduction and meteoroid heat capacity on meteoric ablation. *Monthly Notices of the Royal Astronomical Society* 133:411–420.

Klein P. H. 1967. Thermal conductivity, diffusivity, and specific heat of calcium tungstate from 77° to 300° K. In *Thermal conductivity: Proceedings of the seventh conference*, edited by Flynn D. R. and Peavy B. A. Washington, D.C.: United States National Bureau of Standards. *NBS Special Publication* 302:399–402.

Macke R. J., Consolmagno G. J., and Britt D. T. 2014. Heat capacities of ordinary chondrites. LPI Contribution 1800. Houston, Texas: Lunar and Planetary Institute. 5046 p.

Matsui T. and Osako M. 1979. Thermal property measurement of Yamato meteorites. *Memoirs of National Institute of Polar Research Special Issue* 15:243–252.

Monte C., Becker M., Hollandt J., Manara J., Arduini-Schuster M., Kabelac S., Conrad R., Greffrath F., Scherer V., Kulenovic R., Linder M., Steinbeck A., and Pfeil R. 2011. Intercomparison "Emissivity of thermal paints" in the temperature range from 100 °C to 800 °C. *European Conference on Thermophysical Properties*, Tessaloniki, Greece, August 28–September 1, 2011.

Opeil C. P., Consolmagno G. J., and Britt D. T. 2010. The thermal conductivity of meteorites: New measurements and analysis. *Icarus* 208:449–454.

Opeil C. P., Consolmagno G. J., Safarik D. J., and Britt D. T. 2012. Stony meteorite thermal properties and their relationship with meteorite chemical and physical states. *Meteoritics & Planetary Science* 47:319–329.

Parker W. J., Jeninks R. J., Butler C. P., and Abbott G. L. 1961. Flash method of determining thermal diffusivity, heat capacity, and thermal conductivity. *Journal of Applied Physics* 32:1679–1684.

Parthasarathy G. and Sharma S. R. 2004. High-temperature electrical and thermal properties of Burdett, Dalhart, Faucet and Wellman ordinary chondrites. *Current Science* 109:1366–1368.

Popova O. P., Jenniskens P., Emel'yanenko V., Kartashova A., Biryukov E., Khaibrakhmanov S., Shuvalov V., Rybnov Y., Dudorov A., Grokhovsky V. I., Badyukov D. D., Yin Q.-Z., Gural P. S., Albers J., Granvik M., Evers L. G., Kuiper J., Kharlamov V., Solovyov A., Rusakov Y. S., Korotkiy S., Serdyuk I., Korochantsev A. V., Larionov M. Y., Glazachev D., Mayer A. E., Gisler G., Gladkovsky S. V., Wimpenny J., Sanborn M. E., Yamakawa A., Verosub K., Rowland D. J., Roeske S., Botto N. W., Friedrich J. M., Zolensky M., Le L., Ross D., Ziegler K., Nakamura T., Ahn I., Lee J. I., Zhou Q., Li X.-H., Li Q.-L., Liu Y., Tang G.-Q., Hiroi T., Sears D., Weinstein I. A., Vokhmintsev A. S., Ishchenko A. V., Schmitt-Kopplin P., Hertkorn N., Nagao K., Haba M. K., Komatsu M., and Mikouchi T. 2013. Chelyabinsk airburst, damage assessment, meteorite recovery, and characterization. *Science* 342:1069–1073.

Robie R. A., Hemingway B. S., and Fisher J. R. 1978. *Thermodynamic properties of minerals and related substances at 298.15 K and 1 bar pressure and at higher temperature*. U.S. Geological Survey Bulletin. 1452. Washington, D.C.: US Government Printing Office. 455 p.

Rudee M. L. and Herndon J. M. 1981. Thermal history of the Abee enstatite chondrite II; Thermal measurements and heat flow calculations. *Meteoritics & Planetary Science* 342:134–140.

Scheirich P., Durech J., Pravec P., Kozubal M., Dantowitz R., Kaasalainen M., Betzler A. S., Beltrame P., Muler G., Birtwhistle P., and Kugel F. 2010. The shape and rotation of asteroid 2008 TC3. *Meteoritics & Planetary Science* 45:1804–1811. doi:10.1111/j.1945-5100.2010.01146.x.

Schuessler M., Auweter-Kurtz M., Herdrich G., and Lein S. 2009. Surface characterization of metallic and ceramic TPS-materials for reusable space vehicles. *Acta Astronautica* 65:676–686.

Shaddad M. H., Jenniskens P., Numan D., Kudoda A. M., Elsir S., Riyad I. F., Ali A. E., Alameen M., Alameen N. M., Eid O., Osman A. T., AbuBaker M. I., Yousif M., Chesley S. R., Chodas P. W., Albers J., Edwars W. N., Brown P. G., Kuiper J., and Friedrich J. M. 2010. The recovery of asteroid 2008 TC_3. *Meteoritics & Planetary Science* 45:1557–1589.

Szurgot M. 2011. On the specific heat capacity of meteorites (abstract #1150). 42nd Lunar and Planetary Science Conference. CD-ROM.

Wach R. A., Szurgot M., and Matusiak M. 2014. Thermal properties of Kilabo chondrite (abstract #5010). 77th Annual Meteoritical Society Meeting Meteoritics & Planetary Science 49.

Yomogida K. and Matsui T. 1983. Physical properties of ordinary chondrites. *Journal of Geophysical Research* 88:9513–9533.

Zolensky M., Herrin J., Mikouchi T., Ohsumi K., Friedrich J., Steele A., Rumble D., Fries M., Sandford S., Milam S., Hagiya K., Takeda H., Satake W., Kurihara T., Colbert M., Hanna R., Maisano J., Ketcham R., Goodrich C., Le L., Robinson G.-A., Martinez J., Ross K., Jenniskens P., and Shaddad M. 2010. Mineralogy and petrography of the Almahata Sitta ureilite. *Meteoritics & Planetary Science* 45:1618–1637.